Supplementary Material (ESI) for Chemical Communications

Electronic Supplementary Information

First (3,6)-connected framework constructed from sandwich-type polyoxometalate building blocks containing novel octa-copper cluster

Jun-Wei Zhao, Jie Zhang, Shou-Tian Zheng and Guo-Yu Yang*

State Key Laboratory of Structural Chemistry, Fujian Institute of Research on the Structure of Matter and Graduate School of the Chinese Academy of Sciences, Fuzhou, Fujian 350002, P. R. China. E-mail: ygy@fjirsm.ac.cn; Fax: (+86) 591-83710051

1. Synthetic discussion:

To date, a large number of the purely inorganic *d*-block transition-metal-encapsulated sandwich-type polyoxometalates (POMs) have been obtained using di-, tri- or even multi-vacant POM precursors by conventional aqueous solution method under atmosphere pressure, especially for the Keggin-/Dawson-type polyoxotungstate derivatives. However, this approach was not applied to make inorganic-organic composite octa-copper sandwiched polyoxotungstates in the presence of amines. Therefore, we utilized hydrothermal method to investigate this subject. Hydrothermal conditions are able to make a reaction shift from thermodynamic to kinetic so that equilibrium phases are replaced by structurally more complicated meta-stable phases.[1] Under hydrothermal environment, the reduced viscosity of the solvent enhances reaction reactivity of complicated meta-stable phases and further results in the enhanced rates of solvent extraction of solids and crystal growth from solution. Since the different solubility problems can be minimized, a variety of organic and inorganic components can be introduced.[1c] At the beginning of our work, a novel hexa-Cu^{II} sandwiched silicotungstate $[Cu(dap)_2]_2\{[Cu(dap)_2(H_2O)]_2[Cu_6(dap)_2(\alpha\text{-B-}SiW_9O_{34})_2]\}\cdot 4H_2O$ (**2**) was firstly isolated.[2] As a continuance of the work, we also isolated a dark-green unprecedented inorganic-organic composite germanotungstate $Cu(H_2O)_2H_2[Cu_8(dap)_4(H_2O)_2(\alpha\text{-B-}GeW_9O_{34})_2]$ (**1**) by reaction of trivacant Keggin precursor α-A-GeW_9 with the Cu^{2+} cations in the presence of 1,2-diaminopropane. Different from **2**, **1** is an octa-copper sandwiched germanotungstate with the 3-D network. Under the similar conditions to **1**, we again obtained another octa-copper sandwiched silicotungstate with the 3-D network $[Cu(H_2O)_2]H_2[Cu_8(en)_4(H_2O)_2(\alpha\text{-B-}SiW_9O_{34})_2]$ (**3**) (en = ethylenediamine), which is nearly isostructural to **1** (Fig. S12). Unfortunately, the similar octa-copper sandwiched phosphotungstate is not separated until now. When using 1,6-diaminohexane (dah), triethylenetetramine (teta) or tetraethylenepentamine (tepa) in place of en, dap or deta in the aforementioned system, only amorphous powders were afforded. Therefore, the sizes of amines play an important role in the structural constructions.

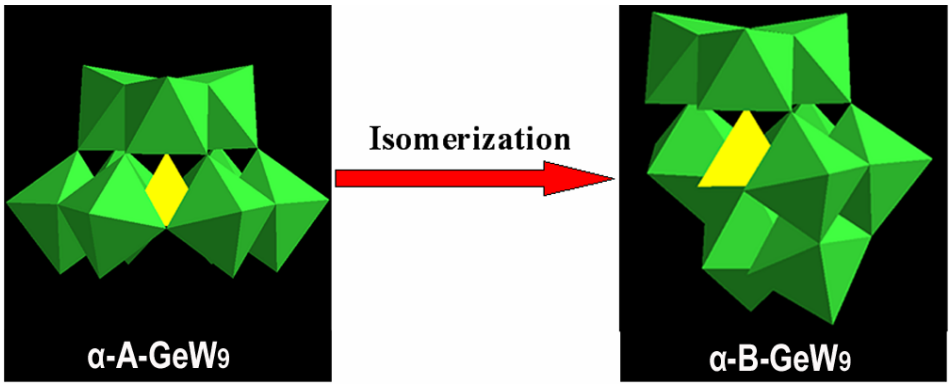

Scheme S1. The isomerization transformation of α-A-GeW_9 and α-B-GeW_9.

Notice that it is necessary that the transformation between different isomers occurred in the formation of **1, 2** and **3**, both experienced the following reaction procedures: isomerization (α-A-XW_9 → α-B-XW_9) (X = Si and Ge) (**Scheme S1**), copper incorporation and polymerization. The isomerization transformation of α-A-GeW_9 and α-B-GeW_9 was previously observed.[3] For example, in 2004, when Kortz et al. reacted α-A-GeW_9 with Cu^{2+}, Mn^{2+}, Zn^{2+} and Cd^{2+} ions to construct the sandwich-type germanotungstates $[M_4(H_2O)_2(\alpha\text{-B-}GeW_9O_{34})_2]^{12-}$, they already observed the occurrence of the isomerization of α-A-GeW_9 → α-B-GeW_9 during the course of the reaction in an aqueous acidic medium upon heating.[3] This isomerization of α-A-XW_9 → α-B-XW_9 may be closely related to the reaction conditions and the stability of the resulting compounds. On one hand, when the reaction is carried out under heating condition, it is favorable for this isomerization ofα-A-XW_9 → α-B-XW_9,[3,4] which is in good agreement with the driving force of isomerization controlled by the thermodynamic factors.[4b,c] On the other hand, the α-A-XW_9 unit has six exposed surface oxygen atoms in the vacant site, while the α-B-XW_9 unit has seven exposed surface oxygen atoms in the vacant site (**Scheme S1**), therefore, the α-B-GeW_9 unit can work as a heptadentate ligand to coordinate to the *in-situ* generated octa-copper clusters and further enhance the stability of the resulting compounds.

1. (a) J. Gopalakrishnan, *Chem. Mater.* 1995, **7**, 1265; (b) D. Hagrman, C. Sangregorio, C. J. O'Connor and J. Zubieta, *J. Chem. Soc. Dalton Trans.* 1998, 3707; (c) H. Jin, Y. Qi, E. Wang, Y. Li, C. Qin, X. Wang and S. Chang, *Eur. J. Inorg. Chem.* 2006, 4541.
2. S.-T. Zheng, D.-Q. Yuan, J. Zhang and G.-Y. Yang, *Inorg. Chem.*, 2007, **46**, 4569.
3. U. Kortz, S. Nellutla, A. C. Stowe, N. S. Dalal, U. Rauwald, W. Danquah and D. Ravot, *Inorg. Chem.*, 2004, **43**, 2308.

4. (a) W. H. Knoth, P. J. Domaille and R. L. Harlow. *Inorg. Chem*. 1986, **25**, 1577; (b) U. Kortz, I. M. Mbomekalle, B. Keita, L. Nadjo and P. Berthet. *Inorg. Chem.* 2002, **41**, 6412; (c) P. J. Domaille, *Inorg. Synth.* John Wiley & Sons: New York, 1990, **27**, 96.

2. Discussion on Jahn-Teller (JT) effect of CuX_6 octahedra and *pseudo*-Jahn-Teller (PJT) effect of CuX_5 square pyramids:

In **1**, it is of interest that there are two kinds of coordination geometries of Cu^{II} ions (six-coordinate octahedral geometry and five-coordinate square pyramidal geometry), therefore, the JT and PJT effects will simultaneously emerge in **1** and result in different isomers or configurations of **1**. As we know, the JT effect is that any non-linear molecular system in a degenerate electronic state will be unstable and will undergo distortion to form a system of lower symmetry and lower energy thereby removing the degeneracy,[1] while the PJT effect is that the vibronic coupling between a degenerate and a non-degenerate state which is induced by a degenerate mode.[2] Therefore, the JT effect is intra-state vibronic coupling while the PJT effect is inter-state vibronic coupling. The JT distortion emerges due to uncompensated forces in the low symmetry charge distribution in any of the degenerate states whereas the PJT distortion is due to the formation of new covalence in the low-symmetry configuration.[3] In the polyatomic system in the high-symmetry configuration, any configuration instability of polyatomic systems is of the JT or PJT vibronic origin. Correspondingly, the JT or PJT vibronic effects are the source of instability of high-symmetry configurations.[2] As for the Cu^{II} system, the JT effect influence the octahedral and square pyramidal geometries, but the PJT effect is only possible for pyramidal geometry. Previously, Bersuker *et al.* used the PJT effect to explain significant differences in stereochemistry of transition-metal MX_5 compounds that differ by the number of *d* electrons only.[4] In the case of **1**, albeit Cu1 and Cu4 ions are five-coordinate, they will have different PJT distortions. The Cu1 ion exhibits the axial elongation (Cu1-O_{eq}: 1.990(7)–2.015(7) Å, Cu1-N_{eq}: 1.975(10)–1.993(10) Å and Cu1-O_{ax}: 2.418(7) Å). On contrast, the Cu4 ion shows the axial compression (Cu4-O_{eq}: 1.85(3)–2.07(4) Å and Cu4-O_{ax}: 1.957 (12) Å). Both Cu2 and Cu3 ions exhibit the axial elongation resulting from the JT effect (Cu2-O_{eq}: 1.979(7)–2.010(7) Å, Cu2-O_{ax}: 2.296(11)–2.392(9) Å; Cu3-O_{eq}: 1.951(7)–1.967(6) Å, Cu3-O_{ax}: 2.446(7) Å). As a result, many possible isomers of **1** may exist. For example, in one of isomers, Cu1/Cu4 ions exhibit the axial compression/elongation, while Cu2 and Cu3 ions still show the axial elongation. Additionally, one copper-substituted POM $[Cu_4K_2(H_2O)_8(\alpha\text{-}AsW_9O_{33})_2]^{8-}$ including simultaneously the axial elongation/compression of Cu^{II} ions, was reported by Kortz *et al.*[5] To date, only an isomorphous silicotungstate has been isolated, and the search of other isomers is on progress.

1. H. A. Jahn and E. Teller, *Proc. Roy. Soc.*, 1937, **A161**, 220.
2. I. B. Bersuker, *Chem. Rev.*, 2001, **101**, 1067.
3. (a) I. B. Bersuker, *The Jahn-Teller Effect and Vibronic Interactions in Modern Chemsitry*; Plenum: New York, 1984; (b) I. B. Bersuker, *Electronic Structure and Properties of Transition Metal Compounds. Introduction to the Theory*; Wiley: New York, 1996.
4. (a) V. Z. Polinger, N. N. Gorinchoy and I. B. Bersuker, *Chem. Phys.*, 1992, **159**, 75; (b) N. N. Gorinchoy, I. B. Bersuker and V. Z. Polinger, *New J. Chem.*, 1993, **17**, 125.
5. U. Kortz, S. Nellutla, A. C. Stowe, N. S. Dalal, J. van Tol and B. S. Bassil, *Inorg. Chem.*, 2004, **43**, 144.

3. Discussion on adsorption experiments of CH_3OH and CH_3CN

We performed the adsorption experiments of **1** in CH_3OH or CH_3CN system for examining whether **1** has the adsorption performance. The specific experimental processes are as follows: **1** (20 mg) was added to CH_3OH or CH_3CN (10 mL). The resulting heterogeneous mixture was kept 24 hours, then filtered and dried for 5 minutes in air. The obtained solids (**1a** and **1b**, respectively) were characterized by IR spectra (Figure S12) and elemental microanalysis. The IR spectrum of **1a** does not show the vibration peak of ν(C-O) of CH_3OH in 1085–1050 cm^{-1}, which indicates **1** can't adsorb CH_3OH. Similarly, the IR spectrum of **1b** also does not show the vibration peak of ν(C≡N) of CH_3CN in 2240–2210 cm^{-1}, which exhibits **1** can't adsorb CH_3CN. The main reason of failure is that the sizes of channels in **1** are too small to accommodate CH_3OH or CH_3CN molecules. The results of elemental microanalyses of **1a** and **1b** do not show the increase of C and H contents, which further confirm that **1** can't adsorb CH_3OH and CH_3CN (The similar measurement method was previously used by Yaghi, *et al.*[1]). The above analysis indicates that there are not real solvent accessible voids in the structure because of too small porous sizes for two types of channels with the cross-section sizes of 2.7 × 2.7 Å and 1.4 × 1.4 Å. The solvent accessible volume of **1** calculated by PLATON[2] is 917 $Å^3$ per unit cell, but the adsorption experiments in CH_3OH and CH_3CN indicate that **1** can't adsorb CH_3OH and CH_3CN. Therefore, there are not real

solvent accessible voids in the structure.

1. (a) H. Li, C. E. Davis, T. L. Groy, D. G. Kelley and O. M. Yaghi, *J. Am. Chem. Soc.*, **1998**, *120*, 2186; (b) H. Li, M. Eddaoudi, D. A. Richardson, O. M. Yaghi, *J. Am. Chem. Soc.*, **1998**, *120*, 8567.
2. A. L. Spek, *PLATON, A Multipurpose Crystallographic Tool*; Utrecht University: Utrecht, The Netherlands, 2001.

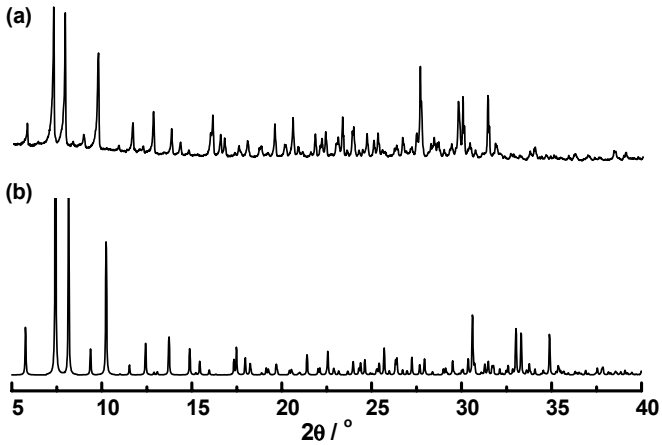

Figure S1. (a) The experimental XRD pattern of the bulk product. (b) The simulated XRD pattern based on the single-crystal solution.

The powder X-ray diffraction pattern of the bulk product is in good agreement with the calculated pattern based on the single-crystal solution, indicating the phase purity of the sample (Fig. S1). The diffraction peaks on both patterns corresponded well in positions, indicating the phase purity of the as-synthesized sample. The intensity difference between the experimental and simulated XRD patterns is due to the variation in preferred orientation of the powder sample during collection of the experimental XRD.

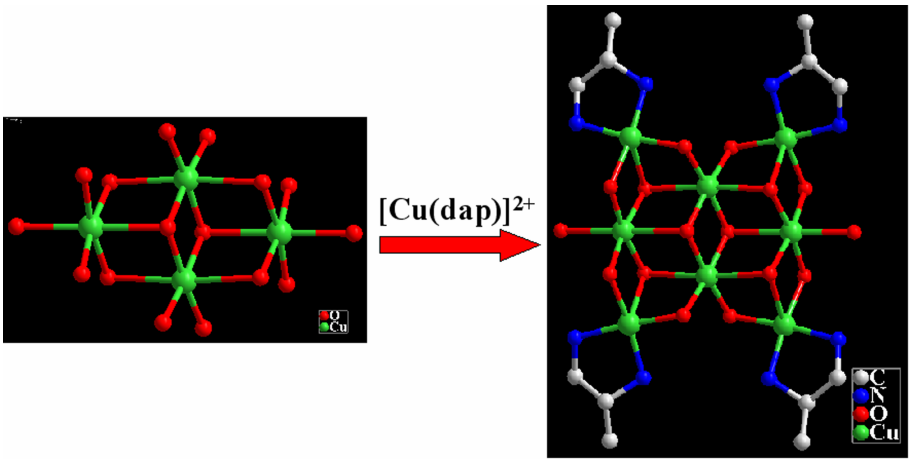

Figure S2. Comparison of tetra-nuclear $\{Cu_4O_{14}(H_2O)_2\}$ cluster in the $[Cu_4(H_2O)_2(\alpha\text{-B-}GeW_9O_{34})_2]^{12-}$ polyoxoanion and octa-nuclear cluster $\{[Cu(dap)]_4Cu_4O_{14}(H_2O)_2\}$ in **1.** The octa-nuclear cluster unit $\{[Cu(dap)]_4Cu_4O_{14}(H_2O)_2\}$ can be visualized that four five-coordinate $[Cu(dap)]^{2+}$ cations are grafted into the four corners of the rhombic $\{Cu_4O_{14}(H_2O)_2\}$ unit via twelve oxygen atoms.

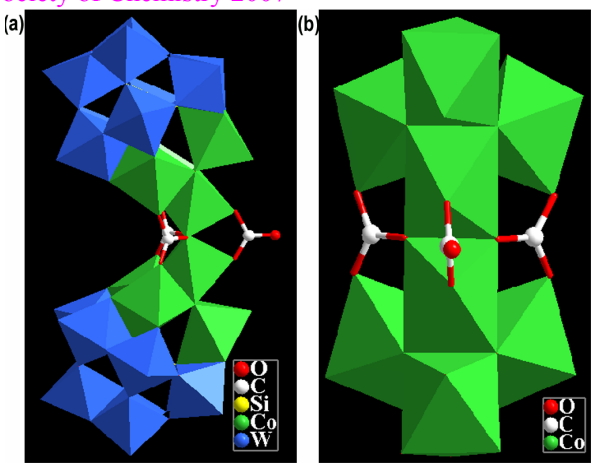

Figure S3. (a) Polyhedral and ball-and-stick representation of $[(\alpha\text{-A-SiW}_9O_{34})_2Co_8(OH)_6(H_2O)_2(CO_3)_3]^{8-}$. (b) Polyhedral and ball-and-stick representation of octa-cobalt^{II} cluster constructed from two $\{Co_4O_9(OH)_3(H_2O)\}$ units through three carbonato groups.

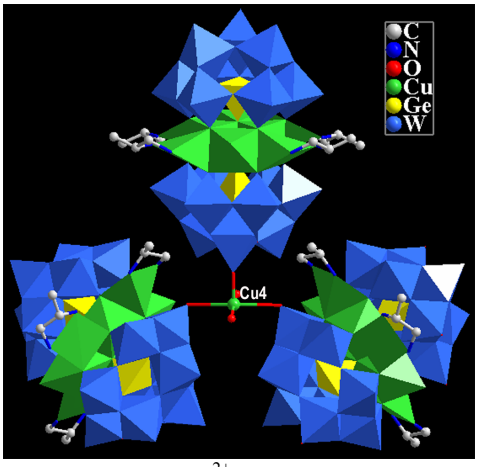

Figure S4. Coordination environment of the $[Cu4(H_2O)_2]^{2+}$ cation, which links three dimeric units $[Cu_8(dap)_4(H_2O)_2(\alpha\text{-B-GeW}_9O_{34})_2]^{4-}$ through three terminal oxygen atoms.

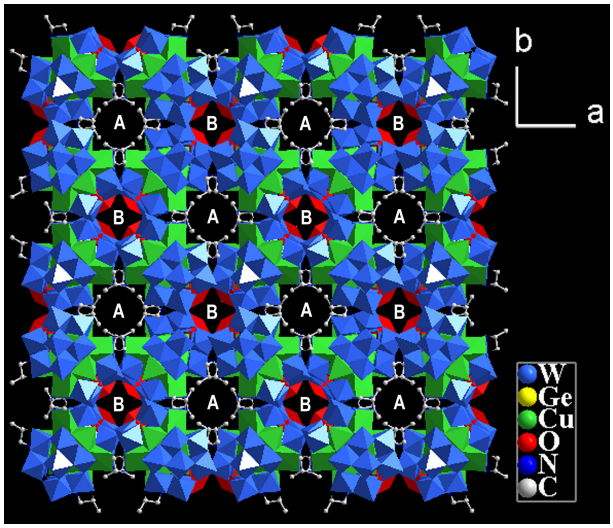

Figure S5. Polyhedral and ball-and-stick representation of 3-D framework viewed down the *c* axis, revealing two types of A and B helical channels. Obviously, the dap ligands and the terminal oxygen atoms form the α-B-GeW_9 fragments protrude into the A channels, while coordination molecules on $[Cu4(H_2O)_2]^{2+}$ ions point to the B channels.

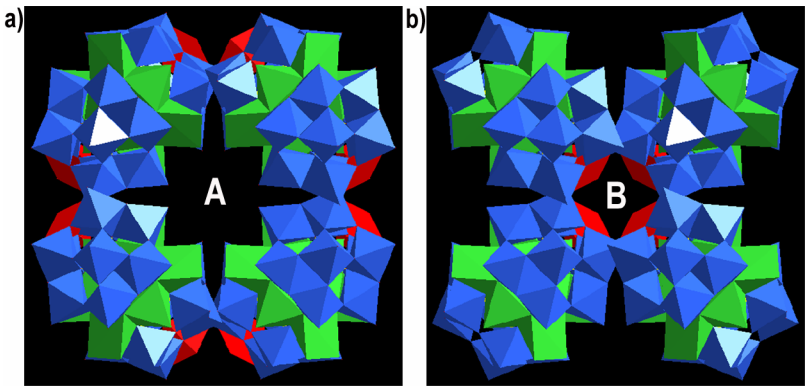

Figure S6. (a) The A channel structure built by the $[Cu_8(dap)_4(H_2O)_2(\alpha\text{-B-}GeW_9O_{34})_2]^{4-}$ units *via* the $[Cu4(H_2O)_2]^{2+}$ bridges. (b) The B channel structure constructed from the $[Cu4(H_2O)_2]^{2+}$ cations *via* the $[Cu_8(dap)_4(H_2O)_2(\alpha\text{-B-}GeW_9O_{34})_2]^{4-}$ units. Highlight: the α-B-GeW_9 units: blue polyhedra; the octa-Cu cluster unit $\{[Cu(dap)]_4Cu_4O_{14}(H_2O)_2\}$: green polyhedra; the $[Cu4(H_2O)_2]^{2+}$ bridges: red polyhedra.

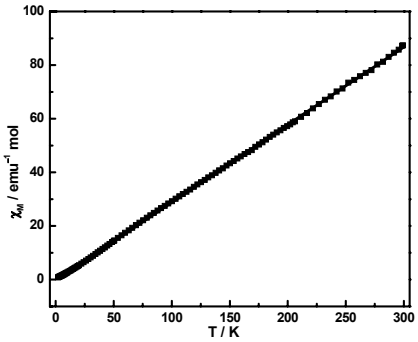

Figure S7. The temperature evolution of the inverse magnetic susceptibility χ_m^{-1} for **1** between 2 and 300 K, and the solid line was generated from the best fit by the Curie-Weiss expression in the range of 2 and 300 K with the Curie constant $C = 3.45$ emu mol^{-1} K and the Weiss constant $\theta = 0.568$ K.

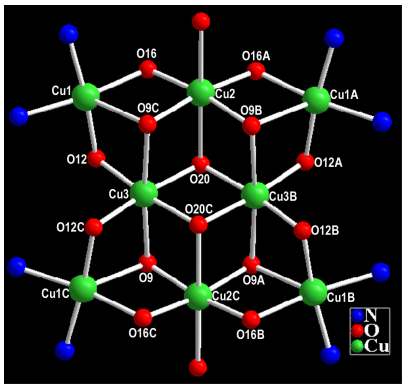

Figure S8. The connection mode of the $\{[Cu(dap)]_4Cu_4O_{14}(H_2O)_2\}$ unit with the partly atom labels. Atoms with "A", "B" and "C" in their labels are symmetry-generated (A: 1/2-y, 1/2-x, z; B: -x, 1-y, -z; C: -1/2+y, 1/2+x, -z).

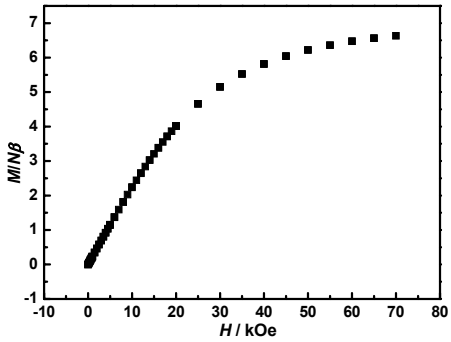

Figure S9. Field dependence of the magnetization of **1**.

Due to the rigidity and size of diamagnetic polyoxoanion frameworks, they impose the geometry of magnetic clusters keeping them well isolated from the neighboring clusters, therefore, this kind of compounds provide a ideal model for the study of exchange interactions in highly symmetrical clusters of high nuclearities and controlled magnetic couplings. Since **1** contains a well-isolated octa-copper^{II} cluster with an unusual geometry and highly symmetrical topology between two diamagnetic polyoxoanion fragments, it is of interest to probe its magnetic property. The temperature dependence of magnetic susceptibility data for **1** is shown in Fig. 3 in the form of $\chi_M T$ versus T. The $\chi_M T$ value corresponds to 3.43 emu mol^{-1} K at 300 K, which is in good consistence with the spin-only contribution (3.38 emu mol^{-1} K) expected for isolated nine Cu^{2+} (S = 1/2) assuming g = 2 per formula unit. As temperature is lowered, the $\chi_M T$ product experiences a gradual rise and reaches a maximum value of 3.84 emu mol^{-1} K at 12 K. This behavior indicates the existence of weak ferromagnetic interactions between Cu^{2+} centers. A sharp drop below the cusp temperature is observed, designating that antiferromagnetic couplings are operative. The inverse magnetic susceptibility data in the temperature range of 2–300 K are fitted to the Curie-Weiss equation with C = 3.454 emu mol^{-1} K (g = 2.02) and θ = 0.568 K (Fig. S7). The small positive Weiss constant (θ) suggests that individual Cu^{2+} spins are weak ferromagnetic interactions in the lattice.

To probe magnetic exchange interactions between Cu^{2+} magnetic centers (Fig. S8), we examine the structural parameters of **1** as shown in Table S1. Because the exchange interactions between the individual Cu^{2+} ions are mediated through the oxo-bridges, it is of importance to identify all the bond lengths and angles of the octa-copper^{II} cluster unit. Since the well-isolated octa-copper^{II} cluster unit employs the C_4 symmetry, there are four types of Cu···Cu distances: 3.18 Å (Cu1···Cu2), 3.11 Å (Cu1···Cu3), 3.22 Å (Cu2-Cu3) and 3.04 Å (Cu3-Cu3B); and seven types of Cu-O-Cu angles: 106.7° (Cu1-O16-Cu2), 91.5° (Cu1-O9C-Cu2), 79.4° (Cu1-O9C-Cu3), 103.2° (Cu1-O12-Cu3), 92.2° (Cu2-O9C-Cu3), 94.9° (Cu2-O20-Cu3) and 101.3° (Cu3-O20-Cu3B). According to the previous study, a classical correlation between the experimental exchange constants and the Cu-O-Cu bond angles (Φ) reveals that the complexes are generally antiferromagnetic for Φ > 98°, while ferromagnetic for Φ < 98°.[1] Because Cu-O-Cu angles vary from 79.4 to 106.7° in **1**, competitive ferromagnetic and antiferromagnetic exchanges will contribute, moreover, the dominant ferromagnetic behavior is expected because the more Cu-O-Cu bond angles are less than 98° in the $\{[Cu(dap)]_4Cu_4O_{14}(H_2O)_2\}$ unit (Table S1).

Table S1. The Cu-O-Cu bond angles (Φ) in the $\{[Cu(dap)]_4Cu_4O_{14}(H_2O)_2\}$ unit of **1**.

	Φ < 98°		Φ > 98°
Cu1-O9C-Cu2	91.5	Cu1-O16-Cu2	106.7
Cu1-O9C-Cu3	79.4	Cu1-O12-Cu3	103.2
Cu2-O9C-Cu3	92.2	Cu2-O16A-Cu1A	106.7
Cu2-O20-Cu3	94.9	Cu1A-O12A-Cu3B	103.2
Cu2-O20-Cu3B	94.9	Cu3-O12C-Cu1C	103.2

Cu2-O9B-Cu3B	92.2	Cu3-O20-Cu3B	101.3
Cu1A-O9B-Cu3B	79.4	Cu3-O20C-Cu3B	101.3
Cu3-O9-Cu1C	79.4	Cu3B-O12B-Cu1B	103.2
Cu3-O9-Cu2C	92.2	Cu1C-O16C-Cu2C	106.7
Cu3-O20C-Cu2C	94.9	Cu2C-O16B-Cu1B	106.7
Cu3B-O20C-Cu2C	94.9		
Cu3B-O9A-Cu2C	92.2		
Cu3B-O9A-Cu1B	79.4		
Cu1C-O9-Cu2C	91.5		
Cu2C-O9A-Cu1B	91.5		

To analyze the observed magnetic property of **1**, a magnetic exchange model has been established for the octa-copper^{II} cluster unit (Fig. 3). The vertices with the numbers 1, 2, 3, 4, 5, 6, 7 and 8 symbolize the copper ions Cu1, Cu2, Cu1A, Cu3, Cu3B, Cu1C, Cu2C and Cu1B. The interactions between Cu1 and Cu2, Cu2 and Cu1A, Cu1C and Cu2C, Cu2C and Cu1B are given by the coupling constant J_1; the interactions between Cu1 and Cu3, Cu1A and Cu3B, Cu1C and Cu3, Cu1B and Cu3B are given by the coupling constant J_2; the interactions between Cu2 and Cu3, Cu2 and Cu3B, Cu2C and Cu3, Cu2C and Cu3B are given by the coupling constant J_3, and the interaction between Cu3 and Cu3B is given by the coupling constant J_4. In the presence of an external magnetic field, the isotropic spin Hamiltonian for the octa-copper^{II} cluster unit is given by:

$$H = -2J_1(S_1S_2 + S_2S_3 + S_6S_7 + S_7S_8) - 2J_2(S_1S_4 + S_3S_5 + S_4S_6 + S_5S_8) - 2J_3(S_2S_4 + S_2S_5 + S_4S_7 + S_5S_7) - 2J_4S_4S_5 \quad (\mathbf{1})$$

Substitution of the eigenvalues of equation 1 into the standard Van Vleck equation yields the expression of the molar magnetic susceptibility (χ_c) of the octa-copper^{II} cluster, as shown in equation 2:[2]

$$\chi_c = (Ng^2\beta^2/3kT)\{\sum S_n^T(S_n^T + 1)(2S_n^T + 1)\exp[-E_n/kT]\}/\{\sum(2S_n^T + 1)\exp[-E_n/kT]\} \quad (\mathbf{2})$$

Here, N is the Avogadro number, K is the Boltzmann constant, T is the temperature in Kelvin, and E_n is the spin exchange energy associated with a spin state S_n^T.

Considering the contribution of a paramagnetic $[Cu4(H_2O)_2]^{2+}$ bridge, the molar magnetic susceptibility (χ) of **1** can be described as equation 3:

$$\chi = \chi_c + (1/2)(3/2)Ng^2\beta^2/3kT \quad (\mathbf{3})$$

Here, the second term refers to the susceptibility of a paramagnetic Cu^{2+} contribution.

To assess the inter-cluster interactions (zJ'), the molecular field correction is considered into the magnetic model, which is consequently represented as $\chi_M = \chi / (1 - zJ'\chi_c/Ng^2\beta^2)$. A more general computational method has been used for this system, such as MAGPACK program package.[3] A best fit with this corrected magnetic susceptibility formula affords magnetic parameters of $J_1 = -2.36$ cm^{-1}, $J_2 = 4.45$ cm^{-1}, $J_3 = 3.03$ cm^{-1}, $J_4 = -2.23$ cm^{-1}, $g = 1.98$ and $zJ' = -0.01$ cm^{-1}. The agreement factor R, defined as $\sum[(\chi_M)_{obs}-(\chi_M)_{cal}]^2/\sum(\chi_M)_{obs}^2$, is equal to 2.52×10^{-4}. These coupling constants prove the above-mentioned classical correlation between the experimental exchange constants and the Cu-O-Cu bond angles. The negative zJ' value accounts for the very small antiferromagnetic phenomenon observed below 12 K. Note that the magnitudes of all J values are comparable, so the octa-copper^{II} cluster in **1** is a frustrated system with many low-lying excited states.[4]

As shown in Fig. S9, the field dependence of the magnetization reveals that the magnetization curve at 2 K increases with raising applied field but its value surprisingly stays smaller than the theoretical value calculated from the Brillouin function for uncoupled nine Cu^{2+} spins. Such behavior may suggest that ferromagnetic interactions ($J_2 > 0$ and $J_3 > 0$) coexist with antiferromagnetic interactions ($J_1 < 0$ and $J_4 < 0$) in the structure. This explanation is ascertained by the fact that the maximum of the $\chi_M T$ value of 3.843 emu mol^{-1} K at 12 K is far smaller than the theoretical expected value of 10.13 emu mol^{-1} K for the ferromagnetic octa-Cu^{II} cluster through oxygen bridges and one isolated paramagnetic Cu^{2+} ion. This phenomenon of the coexistence of competitive ferromagnetic and antiferromagnetic exchanges between Cu^{2+}

magnetic centers in one compound was observed in $K_7Na[Cu_4K_2(H_2O)_6(\alpha\text{-}AsW_9O_{33})_2]\cdot 5.5\ H_2O$.[4]

1 (a) E. Ruiz, P. Alemany, S. Alvarez and J. Cano, *J. Am. Chem. Soc.*, 1997, **119**, 1297; (b) M. P. Shores, B. M. Bartlett and D. G. Nocera, *J. Am. Chem. Soc.,* 2005, **127**, 17986; (c) G. Arom, J. Ribas, P. Gamez, O. Roubeau, H. Kooijman, A. L. Spek, S. Teat, E. MacLean, H. Stoeckli-Evans and J. Reedijk, *Chem. Eur. J.* 2004, **10**, 6476.

2 O. Kahn, *Molecular Magnetism*, VCH, New York, 1993.

3 (a) J. J. Borrás-Almenar, J. M. Clemente-Juan, E. Coronado and B. S. Tsukerblat, *Inorg. Chem.,* 1999, **38**, 6081; (b) J. J. Borrás-Almenar, J. M. Clemente-Juan, E. Coronado and B. S. Tsukerblat, *J. Comput. Chem.,* 2001, **22**, 985.

4 U. Kortz, S. Nellutla, A. C. Stowe, N. S. Dalal, J. van Tol and B. S. Bassil, *Inorg. Chem.*, 2004, **43**, 144.

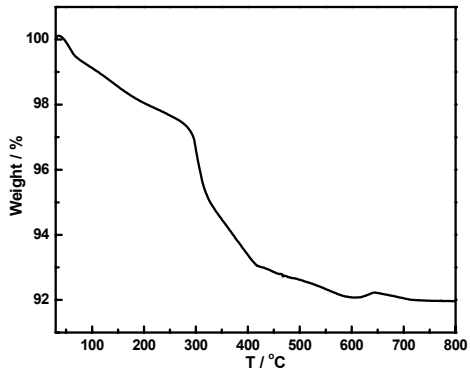

Figure S10. Thermogravimetric (TG) curve of **1** measured in the range of 30–800 ºC under air atmosphere with the heating rate of 10 ºC/min.

The TG curve of **1** shows two steps of weight loss in 30–800ºC (Fig. S10). The first weight loss is 1.52% from 30 to 154ºC, assigned to the release of 4 coordination water molecules (calcd 1.31%), followed by the loss of 6.50% approximating to the removal of 4 dap ligands and the dehydration of 2 protons (calcd 5.74%) from 154 to 800 ºC, meanwhile, the framework collapsed. (Fig. S11)

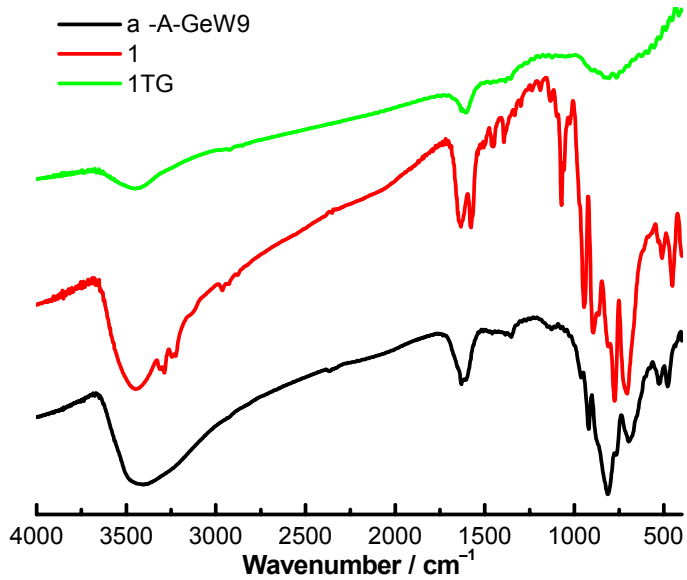

Figure S11. IR spectra of $K_8Na_2[\alpha\text{-}A\text{-}GeW_9O_{34}]\cdot 25H_2O$, **1** and **1TG**. (**1TG** is the product that **1** collapsed at 800 ºC).

The IR spectrum of **1** shows four characteristic vibration bands resulting from the Keggin-type structure, namely, ν(W-O_t), ν(Ge-O_a), ν(W-O_b-W) and ν(W-O_c-W), appearing at 943, 895, 774 and 706 cm^{-1}. In comparison with the spectrum of $K_8Na_2[\alpha\text{-}A\text{-}GeW_9O_{34}]\cdot 25H_2O$, the ν(Ge-O_a) and ν(W-O_b-W) stretching vibration peaks split resulting from a consequence of the lower symmetry of **1**. The stretching bands of the -OH, -NH_2 and -CH_2 groups are observed at 3447 cm^{-1}, 3222–3310 cm^{-1} and 2964 cm^{-1}, respectively. The bending vibration bands of -NH_2 and -CH_2 groups also

appear at 1579 cm^{-1} and 1450 cm^{-1}, respectively. The occurrence of these resonance signals confirms the presence of dap groups, being in good agreement with the single-crystal structural analyses. In comparison with the IR spectrum of **1**, the disappearance of the vibration bands of ν(W-O_b-W) and ν(W-O_c-W) in the IR spectrum of **1TG** indicates that the polyoxoanion framework of **1** collapsed at 800 ºC.

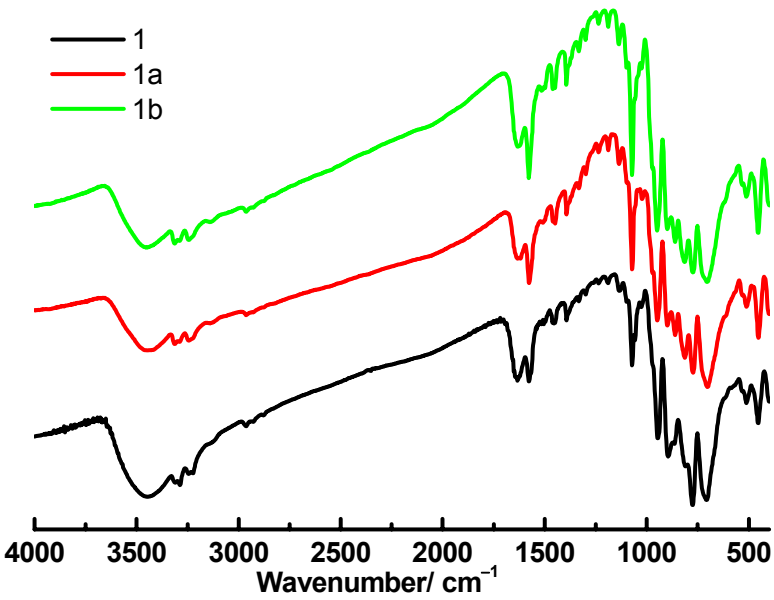

Figure S12. IR spectra of **1, 1a,** and **1b** (**1a** and **1b** for the products kept in CH_3OH and CH_3CN for 24 hours, respectively). The spectra of **1**, **1a** and **1b** are very similar, indicating that no CH_3OH and CH_3CN were adsorbed in the structure of **1**.

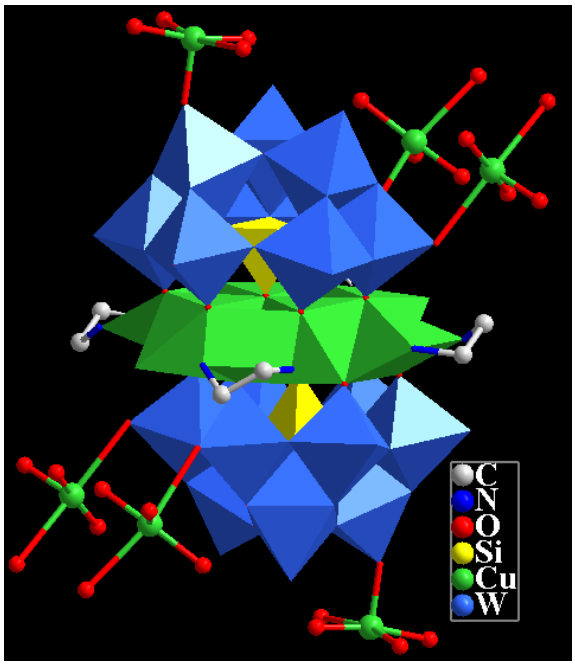

Figure S13. Combined polyhedral/ball-and-stick representation of $[Cu(H_2O)_2]H_2[Cu_8(en)_4(H_2O)_2(\alpha\text{-B-}SiW_9O_{34})_2]$. The hydrogen atoms and lattice water molecules are omitted for clarity.